Journal of Circuits, Systems, and Computers
Vol. 25, No. 10 (2016) 1650123 (18 pages)

DOI: 10.1142/S0218126616501231

Multi-Exposure and Multi-Focus Image Fusion in Gradient Domain*

Sujoy Paul[†,§], Ioana S. Sevcenco[‡,¶] and Panajotis Agathoklis[‡,‖]

[†]*Department of Electrical and Computer Engineering, University of California, Riverside, CA 92521, U.S.A.*

[‡]*Department of Electrical and Computer Engineering, University of Victoria, Victoria, BC V8P 5C2, Canada*
[§]*paul.sujoy.ju@gmail.com*
[¶]*ioana.sevcenco@ece.uvic.ca*
[‖]*pan@ece.uvic.ca*

Received 20 August 2014
Accepted 4 April 2016
Published 8 June 2016

A multi-exposure and multi-focus image fusion algorithm is proposed. The algorithm is developed for color images and is based on blending the gradients of the luminance components of the input images using the maximum gradient magnitude at each pixel location and then obtaining the fused luminance using a Haar wavelet-based image reconstruction technique. This image reconstruction algorithm is of $O(N)$ complexity and includes a Poisson solver at each resolution to eliminate artifacts that may appear due to the nonconservative nature of the resulting gradient. The fused chrominance, on the other hand, is obtained as a weighted mean of the chrominance channels. The particular case of grayscale images is treated as luminance fusion. Experimental results and comparison with other fusion techniques indicate that the proposed algorithm is fast and produces similar or better results than existing techniques for both multi-exposure as well as multi-focus images.

Keywords: Multi-focus image fusion; multi-exposure image fusion; gradient domain image fusion; image reconstruction from gradients.

1. Introduction

In applications such as computer vision, medical imagery, photography and remote sensing, there is a need for algorithms to merge the information acquired by either single or multiple image sensors at the same or different time instants. Generally speaking, image fusion integrates information from a stack of images into a single

*This paper was recommended by Regional Editor Kshirasagar Naik.
¶Corresponding author.

image that has more details than the individual images it is made of. In static image fusion, it is assumed that the input images are aligned and there exist no differences in terms of depth or viewpoint of the imaged scenes. In dynamic image fusion, the imaged scenes in the input images contain some perturbations and are not exactly the same in terms of depth or viewpoint. Many researchers[1,2] tend to first identify the perturbations and then align all the images by image registration to produce a static sequence of images having similar geometry. After registration, the algorithms for static fusion can be applied to these images. There are some algorithms[3] in which the two steps of registration and fusion are integrated. Such algorithms can handle motion of some of the objects in the source images provided that the position of the camera is kept constant.

Static image fusion algorithms can be classified in terms of the way in which the image is processed into pixel-based[3,4] or region-based algorithms.[5,6] In pixel-based methods, the simplest way of obtaining a fused image is by taking a weighted sum at each pixel location, with weights depending on some function of the input images. In region-based techniques, the input images are represented in a multi-resolution framework, using pyramid or wavelet transforms, and then operations such as taking the maximum or averaging the resulting coefficients are used to integrate the information into a more comprehensive image. Naidu[7] proposed a multi-resolution singular value decomposition (SVD)-based image fusion technique. The images to be fused are decomposed into approximation and detail coefficients, a similar structure to that of wavelet decomposition. Then, at each decomposition level, the largest absolute values of the detail coefficients are selected and an average of the approximation coefficients is used to obtain the fused image. Zheng *et al.*[8] proposed a fusion rule based on principal component analysis (PCA) for multi-scale decomposed images. Lewis *et al.*[9] presented a comparative study of pixel- and region-based fusions and indicated that for most cases the region-based techniques provide better results.

Image fusion can be applied to multi-focus or multi-exposure images. In the multi-focus case, the input images are those in which only some portion of the image is well focused, whereas other portions appear blurred. Haghighat *et al.*[10] proposed a multi-focus image fusion technique that operates in the discrete cosine transform (DCT) domain. They compute the variance of the 8×8 DCT coefficients of each image, and the fused blocks are those having the highest variance of DCT coefficients. Song *et al.*[11] proposed a wavelet decomposition-based algorithm for multi-focus image fusion. They fuse the wavelet coefficients using an activity measure which depends on the gradients of the wavelet coefficients. A multiresolution approach was also adopted in the algorithms developed by Li and Wang in Ref. 12 and by Biswas *et al.* in Ref. 13. A survey on multi-focus image fusion techniques can be found in Ref. 14. More recent research[15,16] makes use of edge detection techniques for color image fusion.

In the multi-exposure case, the input images have different exposures. These images have details only in a part of the image while the rest of the image is either

under- or over-exposed. Fusion of such images is done to integrate the details from all images into a single, more comprehensive result. Mertens *et al.*[17] proposed such an algorithm, in which the images are decomposed into Laplacian pyramids and then they are combined at each level using weights depending on the contrast, saturation and well-exposedness of the given images. A technique for image contrast enhancement using image fusion has been presented in Ref. 18 and is similar to Ref. 17. In Ref. 18, the input images to the fusion algorithm are obtained from the original image after applying local and/or global enhancements. Shen *et al.*[19] use a probabilistic model based on local contrast and color consistency to combine multi-exposure images. Li *et al.*[3] fuse the multi-exposure images using a weighted sum methodology based on local contrast, brightness and color dissimilarity. They use a pixel-based method instead of a multi-resolution approach to increase the speed of execution. In Ref. 20, the input images are first divided into blocks and the blocks corresponding to maximum entropy are used to obtain the fused image. The genetic algorithm (GA) is used to optimize block size, and this may require a considerable amount of time to converge.

Image fusion in the gradient domain has been recently studied by some researchers. Socolinsky and Wolff[21] proposed an image fusion approach which integrates information from a multi-spectral image dataset to produce a one band visualization of the image. They generalize image contrast, which is closely related to image gradients, by defining it for multi-spectral images in terms of differential geometry. They use this contrast information to reconstruct the optimal gradient vector field, to produce the fused image. Later, Wang *et al.*[22] fused the images in gradient domain using weights dependent on local variations in intensity of the input images. At each pixel position, they construct an importance-weighted contrast matrix. The square root of the largest eigenvalue of this matrix yields the fused gradient magnitude, and the corresponding eigenvector gives the direction of the fused gradient. Recently, Hara *et al.*[23] used an inter image weighting scheme to optimize the weighted sum of the gradient magnitude and then reconstruct the fused gradients to produce the fused image. The optimization step tends to slow down this technique. Additionally, their technique comprises a manually thresholded intra image weight saliency map, requiring user intervention. An interesting block-based approach was recently proposed by Ma and Wang in Ref. 24. This approach is unique in the way in which it processes color images. Specifically, the RGB color channels of an image are processed together, and instead the images are split into three "conceptually independent components: signal strength, signal structure and mean intensity".[24] This idea was inspired by the increasingly popular structural similarity (SSIM) index,[25] developed by the same main author as an objective measure of similarity between two images.

In this paper, a gradient-based image fusion algorithm is proposed. The algorithm proposed here works for the fusion of both color as well as grayscale images. In the case of color images, one of the key ideas of the fusion algorithm proposed here is that

it treats the luminance and chrominance channels of the images to be fused in a different manner. This different treatment of the channels is motivated by the fact that the luminance channel contains a major part of information about image details and contrast, whereas the chrominance channels contain only color information, to which the human visual system is less sensitive. The fusion of the luminance channels is done in the gradient domain, by taking the gradients with the maximal magnitude of the input images at each pixel location. The luminance channel of the fused image is then obtained by integrating the fused gradients. This done by using a wavelet-based method,[26] which includes a Poisson solver[27] at each resolution. This algorithm is known[28] to produce good results, free from artifacts, when the gradient field is a nonconservative field, as is the case when gradients of different images are combined. Next, for the chrominance part of the color images, fusion is done by taking a weighted sum of the input chrominance channels, with the weights depending on the channel intensities, which conveys information about color. Grayscale images may be dealt with in the same way as the luminance component of color images. The proposed algorithm can be applied for multi-exposure as well as multi-focus images.

The rest of the paper is organized as follows. In Sec. 2, the proposed algorithm is presented. In Sec. 3, experimental results and comparisons with other image fusion algorithms are presented. Finally, in Sec. 4, the main conclusions are drawn.

2. Image Fusion in Gradient Domain

In this section, a new image fusion algorithm is proposed. The proposed algorithm can be applied to fuse together a sequence of either color or grayscale images (minimum two images). A flowchart of the algorithm in its most general case (i.e., fusion of multiple color images) is illustrated in Fig. 1.

The proposed algorithm operates in the YCbCr color space.[a] The luminance (Y) channel represents the image brightness information and it is in this channel where variations and details are most visible, since the human visual system is more sensitive to luminance (Y) than to chrominance (C_b, C_r). This important observation has two main consequences for the proposed fusion algorithm. Firstly, it indicates that the fusion of the luminance and chrominance channels should be done in a different manner, and that it is in the luminance channel where the most advanced part of the fusion is to be performed. Secondly, it reveals that the same procedure used for the luminance channels fusion can be used to fuse single channel images (i.e., images in grayscale representation).

In what follows, the proposed luminance fusion technique is described, followed by chrominance fusion.

[a] Rec. ITU-R BT.601-5, Studio encoding parameters of digital television for standard 4:3 and wide-screen 16:9 aspect ratios, (1982–1986–1990-1992–1994–1995), Section 3.5.

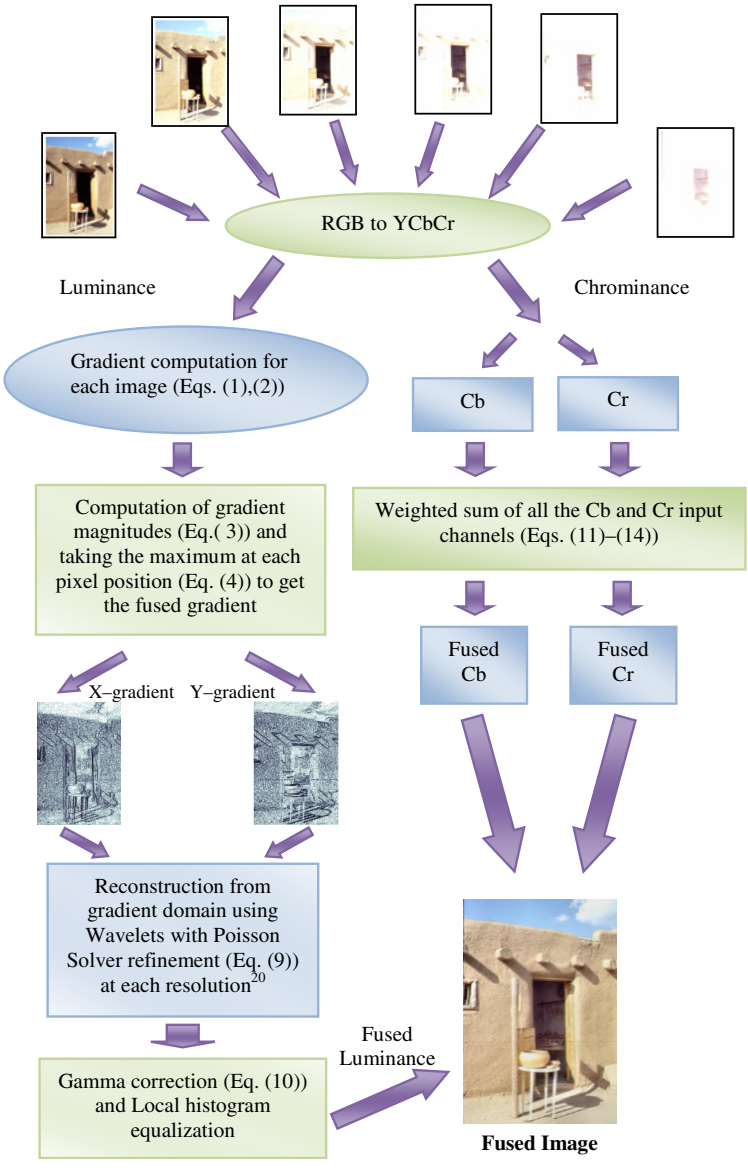

Fig. 1. Flowchart of proposed image fusion algorithm. RGB and YCbCr are color models.[a]

2.1. *Luminance fusion*

As mentioned in the previous sections, the luminance fusion can be carried out on grayscale images, or on color images that are in the YCbCr color coordinate system. If the input images are in RGB representation, conversion to YCbCr should be performed first.

Luminance fusion is performed in the gradient domain. This domain choice is motivated by the fact that the image gradient depicts information on detail content, to which the human visual system is more sensitive under certain illumination conditions. For example, a blurred, over- or under-exposed region in an image will have a much lower gradient magnitude of the luminance channel than the same region in an image with better focus or exposure. This observation implies that taking the gradients with the maximal magnitude at each pixel position will lead to an image which has much more detail than any other image in the stack.

Let the luminance channels of a stack of N input images be $I' = \{I_1, I_2, \ldots, I_N\}$, where $N \geq 2$. According to a commonly employed discretization model, the gradient of the luminance channel of the nth image in the stack may be defined as:

$$\Phi_n^x(x,y) = I_n(x+1,y) - I_n(x,y)\,, \tag{1}$$

$$\Phi_n^y(x,y) = I_n(x,y+1) - I_n(x,y)\,, \tag{2}$$

where Φ_n^x and Φ_n^y are the gradient components in the x- and y-directions. The magnitude of the gradient may be defined as

$$H_n(x,y) = \sqrt{\Phi_n^x(x,y)^2 + \Phi_n^y(x,y)^2}\,. \tag{3}$$

Let the image number having the maximum gradient magnitude at the pixel location (x,y) be $p(x,y)$. It may be mathematically represented as

$$p(x,y) = \max_{1\leq n\leq N} H_n(x,y)\,. \tag{4}$$

Using (4), the fused luminance gradient may be represented as

$$\Phi^x(x,y) = \Phi^x_{p(x,y)}(x,y)\,, \tag{5}$$

$$\Phi^y(x,y) = \Phi^y_{p(x,y)}(x,y)\,, \tag{6}$$

where $\Phi^x_{p(x,y)}(x,y)$ and $\Phi^y_{p(x,y)}(x,y)$ denote the values of the x and y gradient components of the image with index $p(x,y)$, at pixel position (x,y). So, the fused luminance gradient is $\Phi = [\Phi^x, \Phi^y]^T$. It may be noted that the fused luminance gradient has details from all the luminance channels from the stack and in order to get the fused luminance channel, reconstruction is required from the gradient domain. The relationship between the fused gradient (Φ) and the fused luminance channel (I) may be represented as

$$\nabla I = \Phi\,, \tag{7}$$

where $\nabla = [d/dx, d/dy]^T$. We need to solve for I in (7) in order to get the fused luminance, which may not have a solution if the fused gradient violates the zero curl condition. This is due to the fact that the fused gradient is not the gradient of a single

luminance channel, but it is a combination of several luminance gradients. Thus it may not be a conservative field, or in other words, integrals along a closed path may be nonzero. A common approach[29] to solve this problem is to formulate the reconstruction as a $l2$ optimization problem, which leads to solving the Poisson equation,

$$\nabla^2 I = \nabla^T \Phi \,. \tag{8}$$

One way to solve Eq. (8) numerically is by using a large system of linear equations.[29] Some other researchers project the given gradient to another space, in which the zero curl condition is enforced.[30,31] In Ref. 32, a method for gradient integration is presented, where the least square objective function for surface reconstruction is expressed in terms of matrix algebra and it is shown that the minimizer can be obtained as the solution to a Lyapunov equation. In this paper, a gradient reconstruction technique by Sevcenco *et al.*[26] is used. This technique is inspired by Hampton *et al.*[33] and is based on the Haar wavelets. The basic idea of this reconstruction algorithm is the relationship between the Haar wavelet filters and the gradient model. In this technique, the Haar wavelet decomposition coefficients of the luminance channel can be directly computed from the fused luminance gradient. Then, synthesis of these coefficients is done to produce the fused luminance channel. During synthesis, an iterative Poisson solver based on (9) is used at each resolution level to overcome the artifacts that might occur due to the fact that the fused gradients do not satisfy the zero curl condition, as they are from different luminance gradients. The recursion formula may be represented as

$$I(k+1) = I(k) - \frac{1}{4}\left(\begin{bmatrix} -1 & 0 & -1 \\ 0 & 4 & 0 \\ -1 & 0 & -1 \end{bmatrix} \otimes I(k) + \begin{bmatrix} 1 & -1 \\ 1 & -1 \end{bmatrix} \otimes \Phi^x(k) + \begin{bmatrix} 1 & 1 \\ -1 & -1 \end{bmatrix} \otimes \Phi^y(k) \right), \tag{9}$$

where k is the iteration index and $\otimes$ represents 2D convolution. A very small number of iterations are required at each resolution, because a good initial point is provided thus leading to fast convergence. This reconstruction algorithm is based on a modified version of the wavelet transform and, as a result of this, has a low complexity $O(N)$, where N is the number of samples in the signal to be reconstructed. A detailed discussion regarding the computational complexity can be found in Sec. III B of Ref. 33.

After obtaining the image from the gradient domain, some pixels may have intensity values outside the standard range of the luminance component (16/235). This is due to the fact that the fused gradient is obtained by merging multiple image gradients, and as a result, high differences between neighboring gradient values exist,

possibly leading to a reconstructed image with a high dynamic range of pixel intensities. A linear mapping of the pixel intensities of the reconstructed luminance channel can be done such that the resultant intensities lie within the required range. The caveat of this approach, however, is that it leads to a loss of contrast. For this reason, a nonlinear mapping similar to gamma correction is used. The resultant image may be obtained using

$$I(i,j) = \left(\frac{I(i,j) - \min_{i,j} I(i,j)}{\max_{i,j} I(i,j) - \min_{i,j} I(i,j)}\right)^{\gamma} \times R_C + L\,, \tag{10}$$

where $\gamma = \log_e(R_C)/\log_e(R_I)$, R_I is the range of values present in the reconstructed luminance component, $R_C = H - L$ and H and L are the maximum and minimum intensity values in the channel. In the case of the luminance component of a color image, $H = 235$ and $L = 19$, thus $R_C = 216$. After using Eq. (10), the details in the image are preserved and the result does contain more details than the input images. At the end, local histogram equalization[34] is applied on the luminance component. This is done in order to distribute the intensities properly throughout the entire range of display. It may be noted that grayscale images can be fused in the same way as the luminance component of a color image. In case of grayscale images, $H = 255$, $L = 0$, thus $R_C = 255$.

2.2. *Chrominance fusion*

Chrominance fusion is to be carried out for the fusion of the input chrominance channels of color images in YC_bC_r representation (i.e., grayscale images). If the input images are in RGB representation, conversion to YC_bC_r should be performed first, to obtain the luminance (Y) and chrominance (C_b, C_r) channels representation. If the input images are in single channel (e.g., grayscale representation), this step does not apply.

Inherently different than luminance fusion, chrominance fusion operates directly on chrominance values, as opposed to their gradients. Specifically, the chrominance fusion is done by taking a weighted sum of the input chrominance channels. The values in the chrominance channels have a range from 16/240 and carry information about color. These channels are such that when both C_b and C_r are equal to 128, the image is visually similar to a grayscale image, and thus carries the least amount of color information. This motivates selecting the weights for the chrominance channels such that at each pixel position they depend on how far from 128 the chrominance value is. Let us denote the chrominance channels of the input images by $C'_b = \{C_b^1, C_b^2, \ldots, C_b^N\}$ and $C'_r = \{C_r^1, C_r^2, \ldots, C_r^N\}$.

The fused chrominance channels may be represented as follows:

$$C_b(i,j) = \sum_{n=1}^{N} w_b^n(i,j).(C_b^n(i,j) - 128) + 128 \tag{11}$$

where

$$w_b^n(i,j) = \frac{|\, C_b^n(i,j) - 128 \,|}{\sum_{k=1}^{N} |\, C_b^k(i,j) - 128 \,|} \tag{12}$$

$$C_r(i,j) = \sum_{n=1}^{N} w_r^n(i,j).(C_r^n(i,j) - 128) + 128 \tag{13}$$

where

$$w_r^n(i,j) = \frac{|\, C_r^n(i,j) - 128 \,|}{\sum_{k=1}^{N} |\, C_r^k(i,j) - 128 \,|} \tag{14}$$

where $|\cdot|$ returns the absolute value. If all chrominance values at a pixel position in all images from the stack are equal to 128, the corresponding weights will be zero. It may be noted that the fusion of the chrominance channels done by Eqs. (11)–(14) is a pixel-based approach, and is thus less computationally intensive than luminance fusion, which is gradient-based.

3. Performance Evaluation and Comparison

In this section, the performance evaluation of the proposed algorithm on different types of images is presented. The results are compared with the ones of four other image fusion algorithms, namely — DCT,[10] SVD,[7] multi-exposure fusion (MEF)[17] and the gradient weighting (GrW) method.[23] The source codes of the DCT, SVD and MEF methods are available at Refs. 35–37, respectively. The input images used in the comparison are grouped into four different classes according to the type of fusion performed (i.e., multi focus and multi-exposure, grayscale and color) and are presented in the following subsections.

The performance analysis begins with a visual comparison of the results produced by each of the studied algorithms. In passing we note that, to the best of our knowledge, this kind of evaluation (i.e., subjective evaluation) continues to dominate the chart of quality assessment measures for image fusion algorithms. The use of objective measures will be discussed later. The codes for the algorithm proposed in this paper are available at Ref. 38.

3.1. *Multi-focus grayscale images*

Clock and *pepsi*,[35] presented in Figs. 2 and 3, are the two multi-focus grayscale images used for comparison. The fused results produced by the proposed algorithm are presented in Figs. 2(c) and 3(e). For visual comparison, we consider the results using two methods presented in the literature for multi-focus grayscale images, the DCT (Figs. 2(c) and 3(c)) and SVD (Figs. 2(d) and 3(d)) methods. It may be noted in Fig. 2(f), that the DCT method produces undesirable blocking artifacts. The SVD method also produces artifacts that are more clearly visible in Fig. 2(h), on the

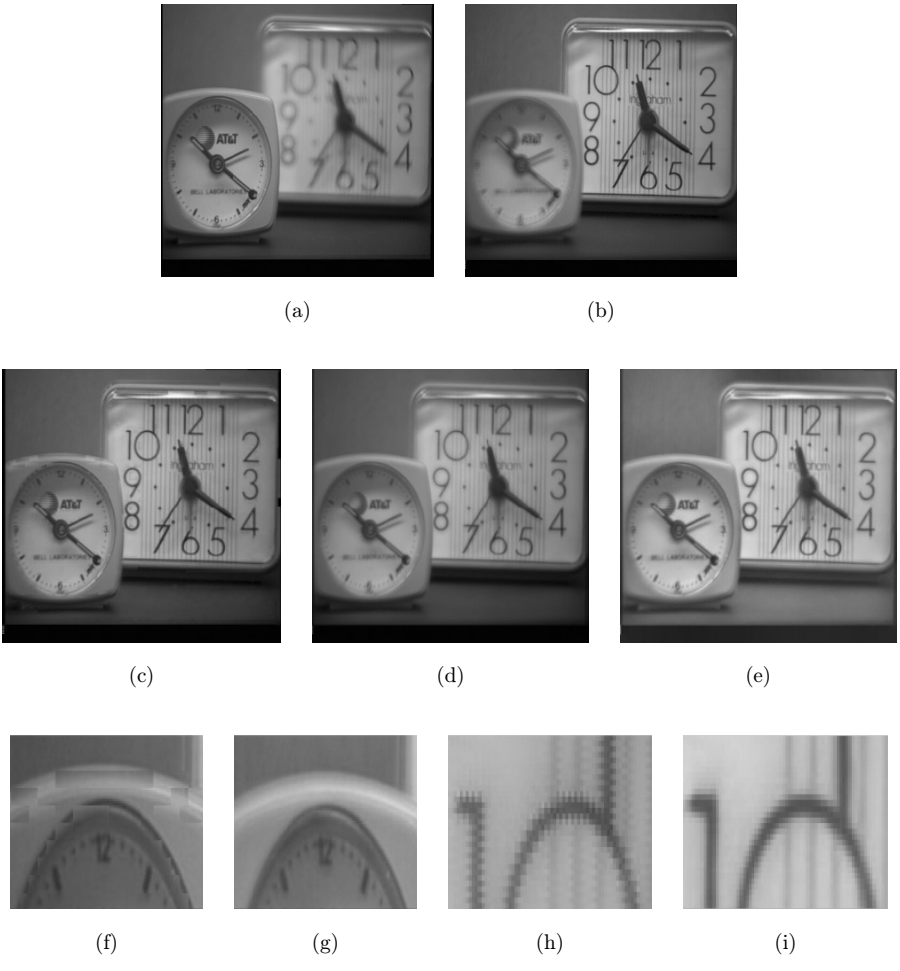

Fig. 2. The 1st row contains the input images (*clock*). The 2nd row contains the fused image by DCT, SVD and proposed algorithm (left to right). (f) and (h) are zoomed in portions of the fused image by DCT and SVD respectively, (g) and (i) are the corresponding zoomed portions of the image fused by proposed algorithm.

zoomed in object edges. On the other hand, the proposed algorithm produces a good fusion of the two multi-focus images and is free from visual artifacts.

3.2. *Multi-focus color images*

Figure 4 presents an example of multi-focus fusion done with the proposed method for a color image named *foot*.[39] None of the four algorithms used here for comparison is proposed by their authors for multi-focus color images and thus the proposed method is not compared to any of them.

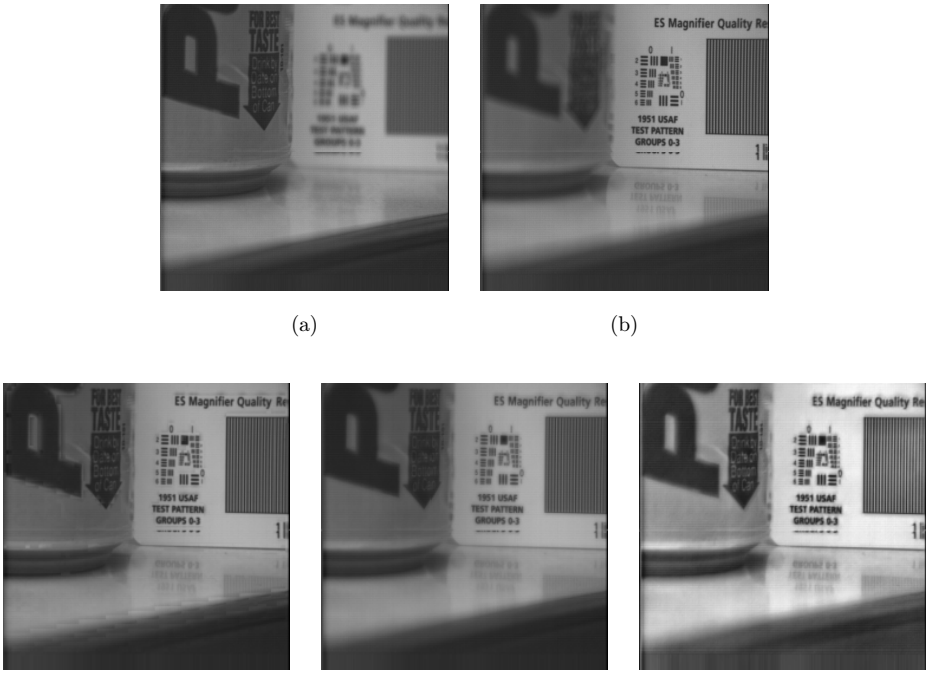

(a) (b)

(c) (d) (e)

Fig. 3. Input images (*pepsi*) are presented in the 1st row. The 2nd row contains the fused image by DCT, SVD and proposed algorithm (left to right).

(a) (b) (c)

Fig. 4. (a) and (b) are the input images (*foot*). The fused result using the proposed algorithm is presented in (c).

3.3. *Multi-exposure grayscale images*

Two multi-exposure grayscale images named *igloo*[40] and *monument*[41] are presented in Figs. 5 and 6. The fused results of the proposed algorithm are presented in Figs. 5(h) and 6(e), respectively. GrW[23] is an algorithm for image fusion, where the

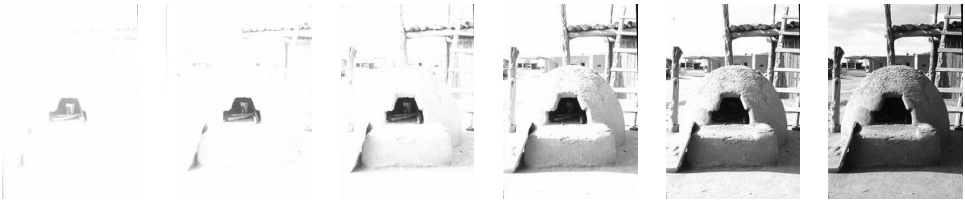

(a) (b) (c) (d) (e) (f)

(g) (h)

Fig. 5. (a)–(f) are the input images (*igloo*). (g) and (h) are the images fused by GrW and the proposed algorithm, respectively.

authors have used multi-exposure grayscale images to test their method. It is a gradient domain fusion method and requires reconstruction to get the fused image. As the authors of the GrW algorithm have not mentioned any specific method for reconstruction, the wavelet-based reconstruction procedure[26] has been used to yield the fused image. The saliency map used by the authors of GrW is not used here, because no automated way of selecting the threshold for the map has been mentioned in their paper. The fused results produced by the GrW method are presented in Figs. 5(g) and 6(d). It may be observed from Fig. 5 that the details inside the igloo building are more visible in the result produced using the method proposed in this paper than in the one produced by the GrW method. Again, in Fig. 6, the sky-cloud portion is more visible in the image fused by the proposed algorithm than in the image fused by the GrW method.

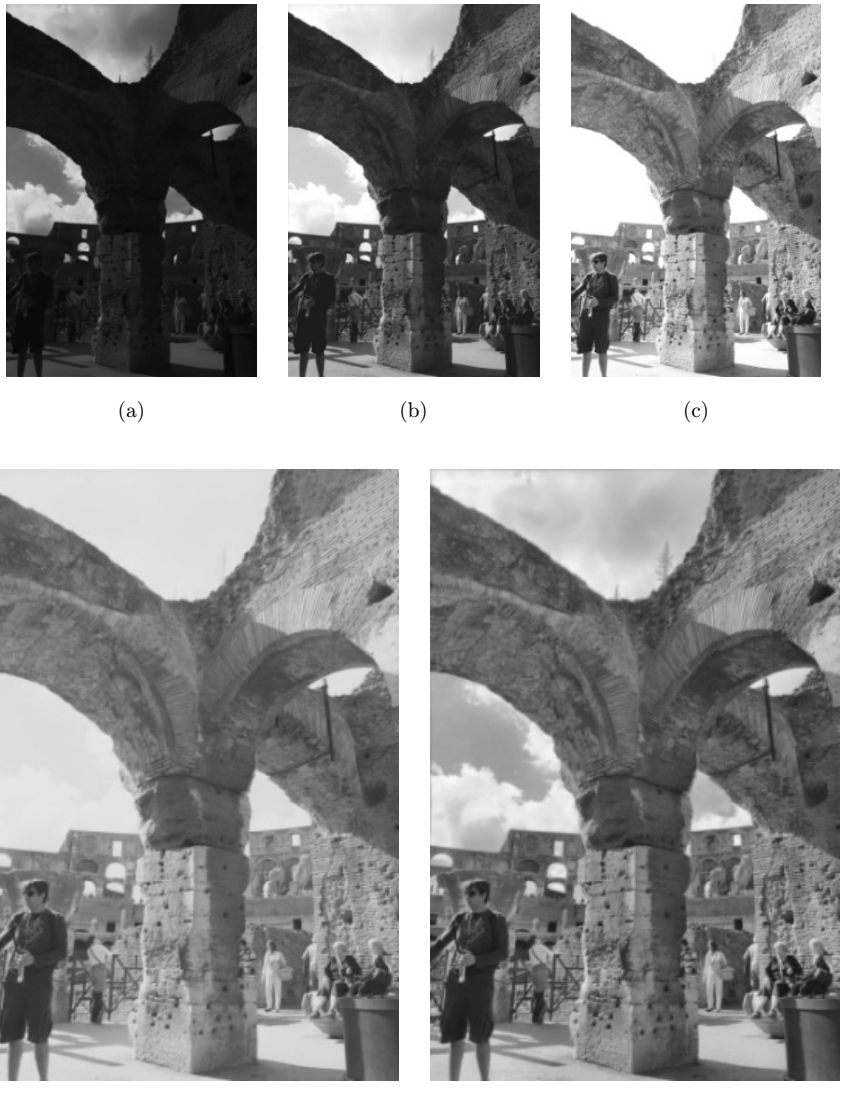

(a) (b) (c)

(d) (e)

Fig. 6. (a)–(c) are the input images (*monument*). (d) and (e) are the images fused by GrW and the proposed algorithm, respectively.

3.4. *Multi-exposure color images*

Door[37] and *house*[37] are the two multi-exposure color images presented in Figs. 7 and 8. It may be observed that for the *door* image, the details within the door are not visible in the first input image and the details outside the door are not visible in the last input image. The proposed algorithm fuses all input images properly, as may be

(a) (b) (c) (d) (e) (f)

(g) (h)

Fig. 7. (a)–(f) are the input images (*door*). (g) and (h) are the fused images by MEF and the proposed algorithm.

observed from the results presented in Figs. 7(h) and 8(f) for the *door* and *house* images, respectively. A technique for MEF for color images presented in the literature is MEF.[17] This method uses a saturation measure defined only for color images. The results produced by the MEF method are presented in Figs. 7(g) and 8(e). It can be seen that the MEF algorithm performs in a similar fashion to the proposed method.

In addition to visual comparison, efforts have been made for quantitative comparison using objective metrics. To the best of our knowledge, in literature there exists no objective quality measure to evaluate the results of image fusion techniques. One of the main reasons behind this appears to be the fact that in most frameworks there exists no ideal fused image that can be used as benchmark. This

Fig. 8. (a)–(d) are the input images (*house*). (e) and (f) are the images fused by MEF and the proposed algorithm, respectively.

has led researchers to develop metrics like edge content (EC),[18,23] second order entropy (SOE),[18] blind image quality (BIQ)[42] and others. These metrics do not require an ideal fused image for comparison, but are prone to give misleading results in the presence of noise and/or blocking artifacts. For example, EC is an average measure of the gradient magnitudes of an image and methods producing blocking artifacts lead to higher EC values. Similar problems are associated with SOE and BIQ, as they are both variations of information and entropy of the image. Thus, we have refrained from comparing the results quantitatively using such metrics.

Comparison with respect to computational time is presented in Table 1 (using Intel® Core™ i3-3110M @ 2.4 GHz and 4 GB RAM). It should be noted that the time presented in the table is normalized with respect to the total number of pixels present in the image and an average over 100 executions of each algorithm. It can be observed that for all images considered, the proposed algorithm consumes the least computational time with respect to the other methods. The filled in entries indicate the average execution times offered by the analyzed algorithms. Specifically, the filled in entries in the DCT and SVD columns represent the times needed to fuse grayscale multi focus images, whereas the filled in entries in the MEF and GrW columns are the times needed to fuse color multi-exposure images, in agreement with the authors' intended applications. The filled in entries in the "proposed method" column represent the average times it took the proposed algorithm to perform grayscale, color, multi-focus or MEF tasks in the same configuration. The entries left

Table 1. Average computational time per pixel ($\times 10^{-4}$ s).

Image name	DCT	SVD	MEF	GrW	Proposed method
Clock	0.0780	0.0556	—	—	0.0224
Pepsi	0.0707	0.0573	—	—	0.0256
Foot	—	—	—	—	0.0134
Door	—	—	0.0650	—	0.0305
House	—	—	0.0296	—	0.0248
Igloo	—	—	—	0.2798	0.0714
Monument	—	—	—	0.1469	0.0340

blank in Table 1 indicate that the respective method was not applied for the respective task.

The results presented in this section indicate that the proposed method performs well for both multi-focus and multi-exposure images, for color as well as for grayscale images. It consistently leads to better and faster results over the other analyzed methods.

4. Conclusion

In this paper, a new gradient-based image fusion algorithm is proposed. Fusion of luminance and chrominance channels is dealt with differently. The fusion of the luminance channel is done in the gradient domain and the fused luminance is obtained using a wavelet-based gradient integration algorithm. The fusion of the chrominance channels is based on a weighted sum of the chrominance channels of the input images. The efficiency of the gradient reconstruction algorithm with complexity $O(N)$ and the simplicity of the chrominance fusion leads to a fast execution speed. Experiments indicate that the proposed algorithm leads to very good results for both multi-exposure as well as multi-focus images.

Acknowledgments

This work was supported by the Natural Sciences and Engineering Research Council of Canada (NSERC) and MITACS.

References

1. J. Hu, O. Gallo, K. Pulli and X. Sun, HDR Deghosting: How to deal with saturation?, *IEEE Conf. Computer Vision and Pattern Recognition*, Portland, Oregon (2013), pp. 1163–1170.
2. G. Xiao, K. Wei and Z. Jing, Improved dynamic image fusion scheme for infrared and visible sequence based on image fusion system, *Int. Conf. Information Fusion* (Cologne, 2008), pp. 1–6.

3. S. Li and X. Kang, Fast multi-exposure image fusion with median filter and recursive filter, *IEEE Trans. Consum. Electron.* **58** (2012) 626–632.
4. M. Kumar and S. Dass, A total variation-based algorithm for pixel-level image fusion, *IEEE Trans. Image Process.* **19** (2009) 2137–2143.
5. J. Yang and R. S. Blum, A region-based image fusion method using the expectation-maximization algorithm, *Annual Conf. Information Sciences and Systems* (Princeton, NJ, 2006), pp. 468–473.
6. P. J. Burt and R. J. Kolczynski, Enhanced image capture through fusion, *Int. Conf. Computer Vision* (Berlin, 1993), pp. 173–182.
7. V. P. S. Naidu, Image fusion technique using multi-resolution singular value decomposition, *Def. Sci. J.* **61** (2011) 479–484.
8. Y. Zheng, X. Hou, T. Bian and Z. Qin, Effective image fusion rules of multi-scale image decomposition, *Int. Symp. Image and Signal Processing and Analysis* (Istanbul, 2007), pp. 362–366.
9. J. J. Lewis, R. J. O'Callaghan, S. G. Bull, D. R., Canagarajah and N. Nikolov, Pixel- and region-based image fusion with complex wavelets, *Inf. Fusion* **8** (2005) 119–130.
10. M. B. A. Haghighat, A. Aghagolzadeh and H. Seyedarabi, Multi-focus image fusion for visual sensor networks in DCT domain, *Comput. Electr. Eng.* **37** (2011) 789–797.
11. Y. Song, M. Li, Q. Li and L. Sun, A new wavelet based multi-focus image fusion scheme and its application on optical microscopy, *IEEE Int. Conf. Robotics and Biomimetics* (Kunming, 2006), pp. 401–405.
12. X. Li and M. Wang, Research of multi-focus image fusion algorithm based on Gabor filter bank, *12th Int. Conf. Signal Processing* (2014), pp. 693–697.
13. B. Biswas, R. Choudhuri, K. N. Dey and A. Chakrabarti, A new multi-focus image fusion method using principal component analysis in shearlet domain, *2nd Int. Conf. Perception and Machine Intelligence* (2015), pp. 92–98, doi 10.1145/2708463.2709064.
14. R. Garg, P. Gupta and H. Kaur, Survey on multi-focus image fusion algorithms, *Recent Adv. Eng. Comput. Sci.* (Chandigarh, 2014), pp. 1–5.
15. Y. Wang, Y. Ye, X. Ran, Y. Wu and X. Shi, A multi-focus color image fusion method based on edge detection, *27th Chinese Control and Decision Conf.* (Qingdao, 2015), pp. 4294–4299.
16. Y. Chen and W.-K. Cham, Edge model based fusion of multi-focus images using matting method, *IEEE Int. Conf. Image Processing* (Quebec City, QC, 2015), pp. 1840–1844.
17. T. Mertens, J. Kautz and F. V. Reeth, Exposure fusion, *Pacific Conf. Computer Graphics and Applications* (2007), pp. 382–390.
18. A. Saleem, A. Beghdadi and B. Boashash, Image fusion based contrast enhancement, *EURASIP J. Image Video Process.* (2012), pp. 1–17.
19. R. Shen, I. Cheng, J. Shi and A. Basu, Generalized random walks for fusion of multi-exposure images, *IEEE Trans. Image Process.* **20** (2011) 3634–3646.
20. J. Kong, R. Wang, Y. Lu, X. Feng and J. Zhang, A novel fusion approach of multi-exposure image, *Int. Conf.* "*Computer as a Tool*", *EUROCON* (Warsaw, 2007), pp. 163–169.
21. D. A. Socolinsky and L. B. Wolff, Multispectral image visualization through first-order fusion, *IEEE Trans. Image Process.* **11** (2002) 923–931.
22. C. Wang, Q. Yang, X. Tang and Z. Ye, Salience preserving image fusion with dynamic range compression, *IEEE Int. Conf. Image Process.* (Atlanta, GA, 2006), pp. 989–992.
23. K. Hara, K. Inoue and K. Urahama, A differentiable approximation approach to contrast-aware image fusion, *IEEE Signal Process. Lett.* **21** (2014) 742–745.
24. K. Ma and Z. Wang, Multi-exposure image fusion: A patch-wise approach, *IEEE Int. Conf. Image Processing* (Quebec City, QC, 2015), pp. 1717–1721.

25. Z. Wang, A. C. Bovik, H. R. Sheikh and E. P. Simoncelli, Image quality assessment: From error visibility to structural similarity, *IEEE Trans. Image Process.* **13** (2004) 600–612.
26. I. S. Sevcenco, P. J. Hampton and P. Agathloklis, A wavelet based method for image reconstruction from gradient data with applications, *Multidimens. Syst. Signal Process.* **26** (2013) 717–737.
27. D. S. Watkins, *Fundamentals of Matrix Computations* (Wiley, New York, USA, 2002).
28. P. J. Hampton and P. Agathoklis, Comparison of Haar wavelet-based and Poisson-based numerical integration techniques, *IEEE Int. Symp. Circuits and Systems*, (Paris, 2010), pp. 1623–1626.
29. R. Lischinski, D. Fattal and M. Werman, Gradient domain high dynamic range compression, *Assoc. Comput. Mach.* **21**(3) (2002), 249–256.
30. R. T. Frankot and R. Chellappa, A method for enforcing integrability in shape from shading algorithms, *IEEE Trans. Pattern Anal. Mach. Intell.* **10** (1988) 439–451.
31. T. Simchony, R. Chellappa and M. Shao, Direct analytical methods for solving Poisson equations in computer vision problems, *IEEE Trans. Pattern Anal. Mach. Intell.* **12** (1990) 435–446.
32. M. Harker and P. O'Leary, Least squares surface reconstruction from measured gradient fields, *IEEE Conf. Computer Vision and Pattern Recognition* (Anchorage, AK, 2008), pp. 1–7.
33. P. J. Hampton, P. Agathoklis and C. Bradley, A new wave-front reconstruction method for adaptive optics system using wavelets, *IEEE J. Sel. Top. Signal Process.* **2** (2008) 781–792.
34. K. Zuiderveld, Contrast limited adaptive histograph equalization, *Graphics Gems IV* (Academic Press Professional, San Diego, 1994), pp. 474–485.
35. M. Haghighat, Multi-focus image fusion in DCT domain (2014). Available at: http://www.mathworks.com/matlabcentral/fileexchange/51947-multi-focus-image-fusion-in-dct-domain. Last accessed: May 21, 2016.
36. V. P. S. Naidu, Image fusion technique using multi-resolution singular value decomposition, *Defence Science Journal* **61**(5) (2011) 479–484, DOI: http://dx.doi.org/10.14429/dsj.61.705, http://www.mathworks.com/matlabcentral/fileexchange/38802-image-fusion-technique-using-multi-resolution-singular-value-decomposition. Last accessed: May 21, 2016.
37. T. Mertens, Data and software implementation of exposure fusion algorithm available by accessing the 'Old Academic Page' tab from http://www.mericam.net/. Last accessed: May 21, 2016.
38. S. Paul, I. Sevcenco, P. Agathoklis, Available at: http://www.mathworks.com/matlabcentral/fileexchange/48782-multi-exposure-and-multi-focus-image-fusion-in-gradient-domain.
39. J. van de Weijer, Image Data Sets, available at: http://lear.inrialpes.fr/people/vandeweijer/data
40. HDR Images from the CAVE (Columbia Automated Vision Environment) Lab-Source exposures courtesy of S. Nayar, available at: http://www.cs.huji.ac.il/∼danix/hdr/pages/columbia.html. Last accessed: May 21, 2016.
41. J. Hu, O. Gallo, K. Pulli and X. Sun, HDR deghosting: How to deal with saturation?, in *IEEE Conf. Computer Vision and Pattern Recognition* (*CVPR*) (Portland, OR, 2013), pp. 1163–1170. Supplementary Material available at: http://users.cs.duke.edu/∼junhu/CVPR2013/
42. S. Gabarda and G. Cristobal, Blind image quality assessment through anisotropy, *J. Opt. Soc. Am. A* **24** (2007) B42–B51.